11th World Congress on Computational Mechanics (WCCM XI)
5th European Conference on Computational Mechanics (ECCM V)
6th European Conference on Computational Fluid Dynamics (ECFD VI)
E. Oñate, J. Oliver and A. Huerta (Eds)

EVALUATION OF A DIFFERENTIAL REYNOLDS STRESS MODEL INCORPORATING NEAR-WALL EFFECTS IN A COMPRESSOR CASCADE TIP-LEAKAGE FLOW

CHRISTIAN MORSBACH*, MARTIN FRANKE† AND FRANCESCA DI MARE*

Institute of Propulsion Technology, German Aerospace Center (DLR)
*Linder Höhe, 51147 Cologne, Germany, †Müller-Breslau-Str. 8, 10623 Berlin, Germany
e-mail: christian.morsbach@dlr.de, martin.franke@dlr.de, francesca.dimare@dlr.de
Web page: http://www.dlr.de/at

Key words: Differential Reynolds Stress Model, Near-Wall Effects, Compressor Cascade, Turbulence Modelling

Abstract. The tip-leakage flow of a low speed compressor cascade at $Ma = 0.07$ and $Re = 400,000$ was simulated employing the Jakirlić/Hanjalić-ω^h (JH-ω^h) differential Reynolds Stress model (DRSM) and results are presented. The predictions are compared with those obtained using the SSG/LRR-ω DRSM and the Menter SST k-ω linear eddy viscosity model (LEVM). In addition to the mean flow quantities, the focus is on the Reynolds stresses and their anisotropy. Both DRSMs show significant improvements compared to the LEVM with respect to the mean flow quantities; however, details of the turbulence structure are more accurately predicted by the JH-ω^h model.

1 INTRODUCTION

The flow in axial compressor rotors is highly complex due to, amongst other phenomena, the vortical motions which develop in the gap between the blades and the machine's casing (tip-gap). Numerical simulations of such flows often rely on highly tuned linear eddy viscosity models (LEVM) despite the high anisotropy which characterises the turbulence field and plays a major role in many phenomena of practical interest. It would appear sensible to adopt, in these cases, an anisotropy-resolving modelling approach. Differential Reynolds stress models (DRSM) belong to this class of closures; however, reports on their application to realistic configurations are scarce. Gerolymos and co-workers were among the first to employ DRSMs to investigate complex configurations, ranging from cascades [1] to multi-stage compressors [2]. Rautaheimo [3] conducted simulations of a centrifugal compressor, whilst Borello et al. [4] investigated the flow through a linear compressor cascade with tip-clearance. In all the above-mentioned studies, results obtained

using DRSMs were found to be superior to those of a LEVM taken as reference, especially for complex 3D flow features. Yet, despite the obvious advantages of DRSMs, they are still not popular in industrial design applications.

In a previous paper, the present authors applied the SSG/LRR-ω DRSM to a compressor cascade flow and compared the results to those obtained with a LEVM and an explicit algebraic Reynolds stress model [5]. It could be shown that the prediction of secondary velocities in the tip-gap flow and the shape of the tip-gap vortex could be improved by the DRSM. However, there was still potential for improvement in the representation of the mean velocities and especially of the Reynolds stresses near the wall. This motivated the present investigation.

2 TURBULENCE MODELLING

In a Reynolds averaged Navier-Stokes (RANS) framework, the objective of turbulence modelling is to determine the Reynolds stress tensor $\overline{\rho u_i'' u_j''}$. This can be accomplished using closures entailing different levels of complexity. For standard industrial CFD applications, the Boussinesq approximation is generally invoked, which defines a turbulent viscosity μ_T to relate the Reynolds stresses directly to the trace-free rate of strain S_{ij}^*. A prominent example of such an approach is the Menter SST k-ω model [6], which will be used as reference in this paper. However, although the linear stress-strain coupling can be justified for certain flow topologies, it cannot be expected to hold in general. In fact, this is the reason for the inability of LEVMs to predict higher order effects such as streamline curvature, rotation or three dimensional boundary layers. In these cases, individual components of the rate of strain tensor influence differently and distinctively the various terms appearing in the Reynolds stress budget, particularly the turbulence production. This mechanism cannot be captured by LEVMs since the production of turbulent kinetic energy in a Boussinesq context relies on the norm of the rate of strain tensor only.

One of the biggest advantages of DRSMs with respect to lower order closures is the exact turbulence production term, which appears in the transport equations for the Reynolds stress tensor derived directly from the Navier-Stokes equations. However, the closure problem is not automatically solved by differential models; it is only shifted, as still higher correlations of fluctuating quantities are introduced. Models have to be found for the dissipation, redistribution due to pressure-strain interaction, and turbulent diffusion of Reynolds stresses. Two differential Reynolds stress models of different complexity will be evaluated in this paper, i. e. the SSG/LRR-ω and the JH-ω^h model.

The SSG/LRR-ω model has been developed specifically in view of application to complex aerodynamic flows. It is a hybrid model in which the quadratic SSG [7] and the linear LRR [8] pressure-strain models are combined. Menter's BSL ω-equation is employed for the scale determining variable along with the blending function F_1. The latter is also used to blend between the LRR model (close to solid walls) and the SSG model (away from walls). For more details on the SSG/LRR-ω model, the interested reader is referred to the original publications by Eisfeld and co-workers [9, 10]. The version used in this study

is documented in [5].

On the other hand, the Jakirlić/Hanjalić model has been developed with particular attention to the exact reproduction of mean flow quantities and turbulent statistics in building block flows. For this purpose, the terms in the Reynolds stress transport equations as well as the dissipation rate equation were calibrated to reproduce the behaviour of their exact counterparts. In particular, using DNS data to compute the model terms, a system of equations was obtained and solved for the unknown model's coefficients. Analysis showed that these can be expressed as functions of turbulence anisotropy invariants and the turbulence Reynolds number [11, 12]. Originally, the model was based on the dissipation rate ϵ. Jakirlić showed that if the homogeneous dissipation rate ϵ^h is used instead, wall limits for the normalised dissipation components are satisfied automatically [13]. While adapting the model to be used in the context of scale-adaptive simulations, Maduta suggested that the specific homogeneous dissipation rate ω^h should be employed [14]. The current model is based on this latest formulation and termed JH-ω^h.

The transport equation for Reynolds stresses in the JH-ω^h model reads:

$$\frac{D\overline{\rho u_i'' u_j''}}{Dt} = \overline{\rho} P_{ij} - \overline{\rho}\epsilon_{ij}^h + \overline{\rho}\left(\Pi_{ij,1} + \Pi_{ij,2} + \Pi_{ij}^w\right) + \frac{\partial}{\partial x_k}\left[\left(\frac{1}{2}\mu + \frac{2C_S}{3C_\mu}\mu_T\right)\frac{\partial \widetilde{u_i'' u_j''}}{\partial x_k}\right] \tag{1}$$

where P_{ij} denotes the production, ϵ_{ij}^h the homogeneous dissipation and Π_{ij} the components of the pressure-strain redistribution term. A simple gradient diffusion (SGD) approach is used to close the turbulent diffusion correlations. Indices occuring twice within a product imply summation over the three spatial directions. As mentioned above, the production term

$$P_{ij} = -\left(\widetilde{u_i'' u_k''}\frac{\partial \tilde{u}_j}{\partial x_k} + \widetilde{u_j'' u_k''}\frac{\partial \tilde{u}_i}{\partial x_k}\right) \tag{2}$$

is exact. The pressure-strain correlation is traditionally split into a slow part $\Pi_{ij,1}$, a rapid part $\Pi_{ij,2}$, and a contribution due to the presence of solid walls Π_{ij}^w. Its components are given by

$$\Pi_{ij,1} = -C_1 \epsilon^h a_{ij} \tag{3}$$

$$\Pi_{ij,2} = k\left[C_3 S_{ij}^* + C_4\left(a_{ip}S_{pj} + a_{jp}S_{pi} - \frac{2}{3}a_{pq}S_{pq}\delta_{ij}\right) + C_5\left(a_{ip}W_{pj} + a_{jp}W_{pi}\right)\right] \tag{4}$$

$$\begin{aligned}\Pi_{ij}^w = {} & C_1^w f_w \frac{\epsilon^h}{k}\left(\widetilde{u_k'' u_m''} n_k n_m \delta_{ij} - \frac{3}{2}\widetilde{u_i'' u_k''} n_k n_j - \frac{3}{2}\widetilde{u_k'' u_j''} n_k n_i\right) \\ & + C_2^w f_w \left(\Pi_{km,2} n_k n_m \delta_{ij} - \frac{3}{2}\Pi_{ik,2} n_k n_j - \frac{3}{2}\Pi_{kj,2} n_k n_i\right).\end{aligned} \tag{5}$$

All closures are formulated in terms of the strain rate and vorticity tensors

$$S_{ij} = \frac{1}{2}\left(\frac{\partial \tilde{u}_i}{\partial x_j} + \frac{\partial \tilde{u}_j}{\partial x_i}\right), \quad S_{ij}^* = S_{ij} - \frac{1}{3}S_{qq}\delta_{ij}, \quad W_{ij} = \frac{1}{2}\left(\frac{\partial \tilde{u}_i}{\partial x_j} - \frac{\partial \tilde{u}_j}{\partial x_i}\right), \tag{6}$$

the Reynolds stress anisotropy tensor

$$a_{ij} = \frac{\widetilde{u_i'' u_j''}}{k} - \frac{2}{3}\delta_{ij} \tag{7}$$

and the wall normal vector $\mathbf{n}$. The influence of the wall is blended by a function dependent on the ratio of the turbulence length scale to the distance to the wall

$$f_w = \min\left[\frac{k^{\frac{3}{2}}}{2.5\epsilon^h y_n}, 1.4\right]. \tag{8}$$

The anisotropy of the dissipation tensor is directly coupled to the anisotropy of the Reynolds stress tensor

$$\epsilon_{ij}^h = \epsilon^h \left[\frac{2}{3}\delta_{ij} + f_s a_{ij}\right] \quad \text{with} \quad f_s = 1 - \sqrt{A}E^2. \tag{9}$$

All model coefficients are functions of invariants of a_{ij} and its dissipation counterpart $e_{ij} = f_s a_{ij}$. The second and third invariants as well as the two-component parameter are given by

$$A_2 = a_{ij}a_{ji}, \quad A_3 = a_{ij}a_{jk}a_{ki} \quad \text{and} \quad A = 1 - \frac{9}{8}(A_2 - A_3) \tag{10}$$

and likewise for the dissipation anisotropy e_{ij}. The coefficients of the JH-ω^h model are summarised in Table 1. In contrast to the SSG/LRR-ω model, all pressure-strain terms are tensorially linear in the anisotropy tensor. The complexity of this model lies in the variable coefficients. In the rapid part of the pressure-strain correlation $\Pi_{ij,2}$ these are chosen so that a classic isotropisation-of-production term with a variable coefficient C_2 is obtained. Furthermore, the model introduces explicit modelling of near-wall effects which Eisfeld's model does not consider.

The homogeneous dissipation rate is related to the specific homogeneous dissipation rate by

$$\epsilon^h = C_\mu k \omega^h \tag{11}$$

with $C_\mu = 0.09$. For this quantity, a transport equation can be derived from the transport equation for ϵ^h. The employed version of the equation

$$\begin{aligned}\frac{D\left(\overline{\rho}\omega^h\right)}{Dt} =& \frac{\partial}{\partial x_i}\left[\left(\frac{1}{2}\mu + \sigma_\omega \mu_T\right)\frac{\partial \omega^h}{\partial x_i}\right] + \alpha\frac{\overline{\rho}\omega^h}{2k}P_{qq} - \beta\overline{\rho}\left(\omega^h\right)^2 \\ &+ \frac{2}{k}\left(\frac{1}{2}\mu + \sigma_d\mu_T\right)\max\left[\frac{\partial\omega^h}{\partial x_i}\frac{\partial k}{\partial x_i}, 0\right] + \frac{C_{\epsilon 3\mu}}{C_\mu}\frac{\widetilde{u_p'' u_q''}}{\epsilon^h}\frac{\partial^2\tilde{u}_i}{\partial x_p \partial x_l}\frac{\partial^2\tilde{u}_i}{\partial x_q \partial x_l}\end{aligned} \tag{12}$$

differs from the exactly transformed version in several aspects. The most important one is the limitation of the cross diffusion term to positive values in analogy to Menter's BSL

Table 1: Coefficients of Reynolds stress and dissipation rate equations.

Model	Coefficient			Model	Coefficient		
$\Pi_{ij,1}$	C_1	$=$	$C+\sqrt{A}E^2$	Π_{ij}^w	C_1^w	$=$	$\max\left[1.0-0.7C, 0.3\right]$
	C	$=$	$2.5AF^{\frac{1}{4}}f$		C_2^w	$=$	$\min\left[A, 0.3\right]$
	F	$=$	$\min\left[0.6, A_2\right]$	Diffusion	C_S	$=$	0.082
	f	$=$	$\min\left[\left(\frac{\mathrm{Re}_T}{150}\right)^{\frac{3}{2}}, 1\right]$	ω^h	α	$=$	0.44
	Re_T	$=$	$\frac{\overline{\rho}k^2}{\mu\epsilon^h}$		β	$=$	0.072
$\Pi_{ij,2}$	C_3	$=$	$\frac{4}{3}C_2$		σ_ω	$=$	0.9091
	C_4	$=$	C_2		σ_d	$=$	0.25
	C_5	$=$	$-C_2$		$C_{\epsilon 3}$	$=$	0.3
	C_2	$=$	$0.8\sqrt{A}$				

equation. This improves stability in complex test cases at the expense of the accuracy of prediction of normal stresses in the viscous sublayer. Evaluation of the turbulent viscosity μ_T in a turbulent plane channel flow resulted in the formulation

$$\mu_T = 0.144A\overline{\rho}k^{\frac{1}{2}}\max\left[10\eta_K, L\right] \quad \text{with} \quad \eta_K = \left(\frac{\nu^3}{\epsilon^h}\right)^{\frac{1}{4}} \quad \text{and} \quad L = \frac{k^{\frac{3}{2}}}{\epsilon^h}. \tag{13}$$

It is used to model the diffusion of the Reynolds stresses and the dissipation rate. In the Navier-Stokes equations it serves a mere numerical stabilisation purpose by increasing the diagonal dominance of the implicit solution matrix [5].

At solid walls the Reynolds stresses vanish as prescribed by the no-slip condition. For the dissipation rate the Taylor microscale is employed to derive the following formulation for ω^h for the first cell away from the wall:

$$\omega^h\big|_{\text{first cell}} = \frac{\nu}{C_\mu y^2}, \quad \left.\frac{\partial\omega^h}{\partial\mathbf{n}}\right|_{\text{wall}} = 0. \tag{14}$$

The gradient is set to zero which is physically incorrect; however, this choice has no influence as long as the diffusion of ω^h is computed using only directly neighbouring cells. This treatment in the JH-ω^h model differs from the SSG/LRR-ω model, where ω is prescribed at the wall according to the suggestion by Menter [15].

3 NUMERICAL METHOD

All computations were performed using the DLR flow solver for turbomachinery applications TRACE. TRACE is a hybrid grid, multi block, compressible, implicit Navier-Stokes code based on the finite volume method. It has been developed for over 20 years

at the DLR Institute of Propulsion Technology and is designed to meet the specific requirements of simulating turbomachinery flows [16]. Within the RANS framework, the turbulence transport equations are solved with a second-order accurate, conservative, segregated solution method [17]. The source terms for the Reynolds stresses and dissipation rate are linearised and treated implicitly [5]. Due to the low Mach number of the compressor test case, a local low Mach preconditioning of the type proposed by Turkel was employed [18].

A key to a more robust solution method was the introduction of explicit realisability constraints for all six Reynolds stress tensor components, as theoretically investigated by Schumann [19]. Since the Reynolds stress equations are solved in a segregated manner, it is possible that one of the normal components $\widetilde{u''_\alpha u''_\alpha}$ (no summation over Greek indices) violates the realisability condition of positive normal stresses. This limit is explicitly enforced; however, it is also very important to satisfy the constraints on the shear stresses resulting from the Cauchy-Schwarz inequality as otherwise the production term of Reynolds stresses would yield unphysical values which could lead to a diverging solution. Therefore, the shear stresses are also limited based on the limited normal stresses.

4 RESULTS

The implemented DRSMs were validated using a series of building block flows. In this work, the results of the simulations of the turbulent flow in a plane channel are reported as an example. Figure 1 shows the results at Reynolds numbers based on friction velocity of $Re_\tau = 180$ [20] and $Re_\tau = 2003$ [21]. All quantities are made non-dimensional by the friction velocity u_τ. The velocity profile is predicted to a similar degree of accuracy by the Menter SST k-ω and the SSG/LRR-ω models. Especially the prediction of the logarithmic region at y^+ towards the channel centre line is improved by the JH-ω^h model. Great improvements can be seen in the reproduction of the wall-normal velocity fluctuation v^+ and the streamwise velocity fluctuation u^+. The JH-ω^h model is able to qualitatively capture the peak in u^+. On the other hand, quantitative agreement including the asymptotic behaviour towards the wall is not as well achieved as it is by the original JH-ϵ model [22].

The low speed compressor cascade investigated experimentally by Muthanna [23] and Tang [24] (operated at $Ma = 0.07$ and $Re = 400,000$) is representative of a turbomachinery flow, characterised by complex 3D flow features. A detailed description of the numerical setup was given in [5]. For all turbulence models tested in this work the same inflow boundary conditions, i.e. isotropic turbulence, were used. The pressure distribution on the blade at midspan, predicted by the different turbulence models, lies within the experimental scatter, confirming that the boundary conditions were chosen correctly. An overview of the flow topology is shown in Figure 2. The flow through the tip-gap of 1.65% blade height leads to the development of the tip-gap vortex visualised by the streamlines. Qualitatively the velocity deficit in the vortex core predicted with the JH-ω^h model is compared to the measured data at $x/c_a = 0.98$, c_a being the axial chord length.

Muthanna determined the centre of the vortex as the location of the maximal stream-

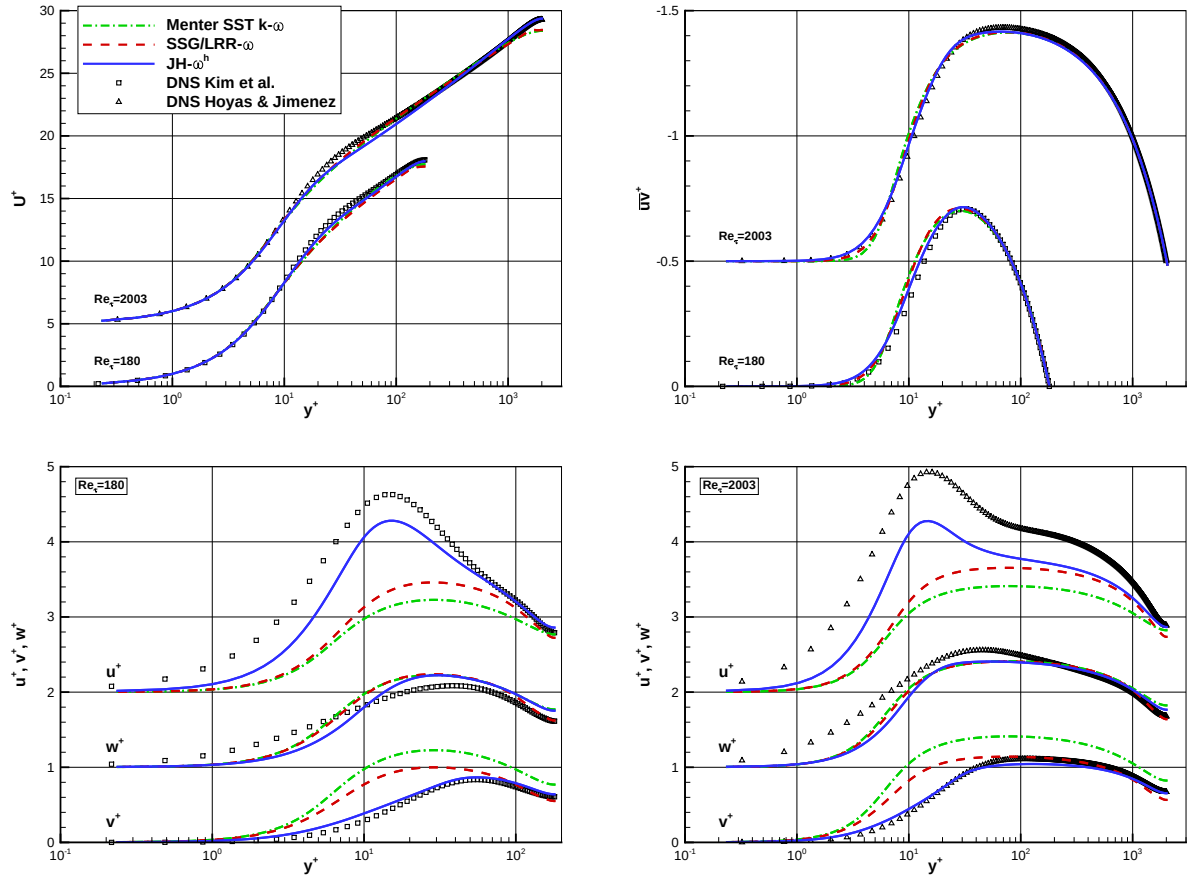

Figure 1: Turbulent plane channel flow at $Re_\tau = 180$ [20] and $Re_\tau = 2003$ [21]. Normalised velocity profile, shear stress and normal stresses are compared for Menter SST k-ω, SSG/LRR-ω and JH-ω^h turbulence models.

wise vorticity [23]. From the simulation data, the vortex core was determined using the λ_2 criterion. The position of the vortex core (spheres) at four measurement planes is shown in Figure 3. To facilitate comparison, its path is also projected onto the side wall (corresponding lines without symbols). From these results it can be argued that none of the employed turbulence models shows a clear advantage over the others and that all of them predict a path that is comparable to the experiment.

Tang measured the mean velocities and Reynolds stresses at various stations in the tip-gap [24]. Due to space constraints, only the station 5c was selected to be shown in this paper as the most representative, with its location illustrated in Figure 3. To obtain a representation which is independent of the selected coordinate system, invariants of the Reynolds stress anisotropy tensor a_{ij}, given by equation (10), are plotted in Figure 4 instead of Reynolds stress tensor components. Close to a solid wall, turbulence is expected to tend towards the two-component limit with $A = 0$. Towards the end wall, experiments

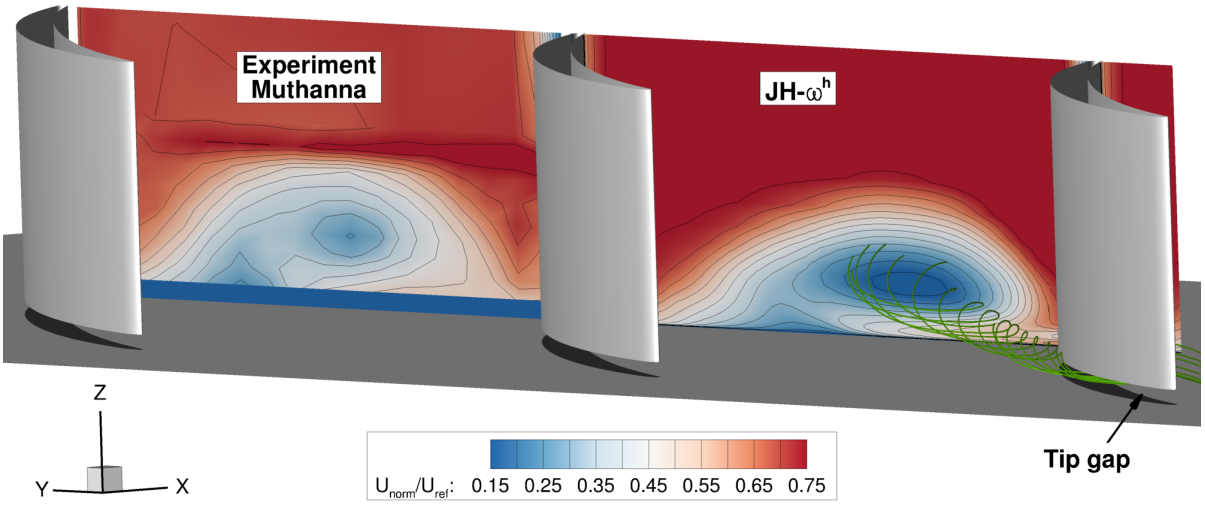

Figure 2: Illustration of tip-leakage flow in the Virginia Tech compressor cascade. Measured mean velocity in blade passage is compared to prediction by JH-ω^h DRSM.

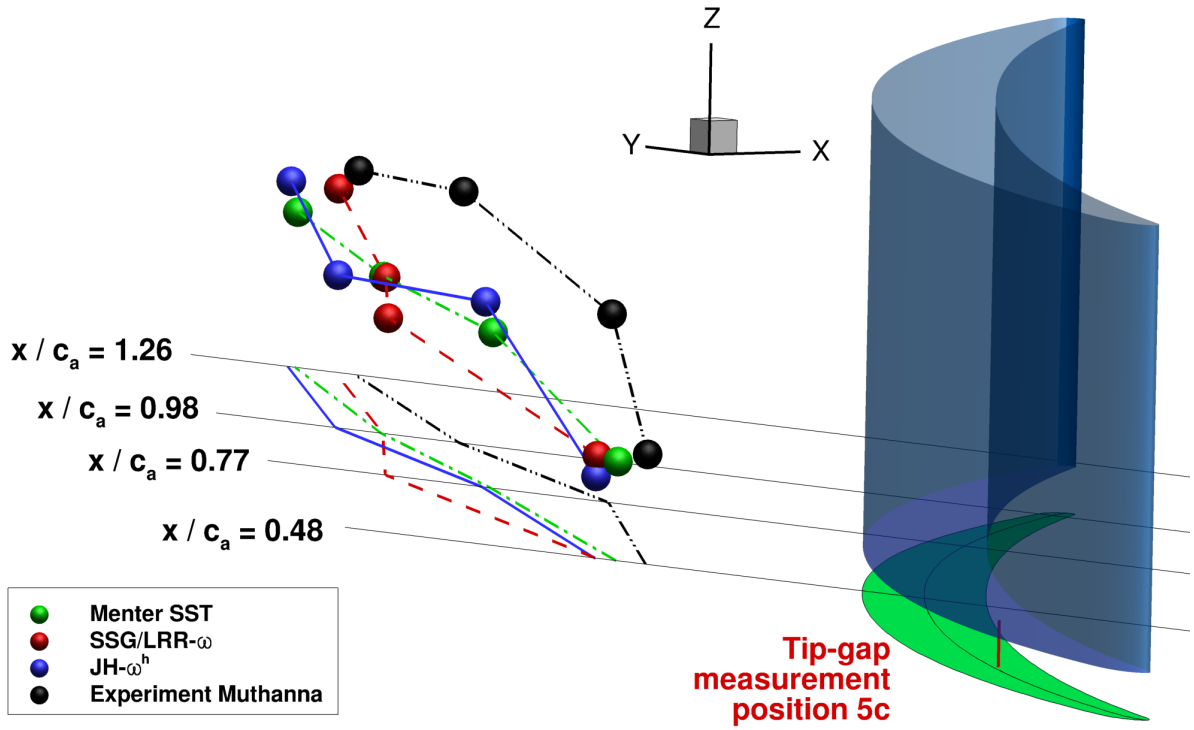

Figure 3: Prediction of tip-gap vortex centre. Spheres represent vortex centre at different measurement planes. Trajectory is projected to x-y plane for better comparability. Position for examined tip-gap measurements is shown in red.

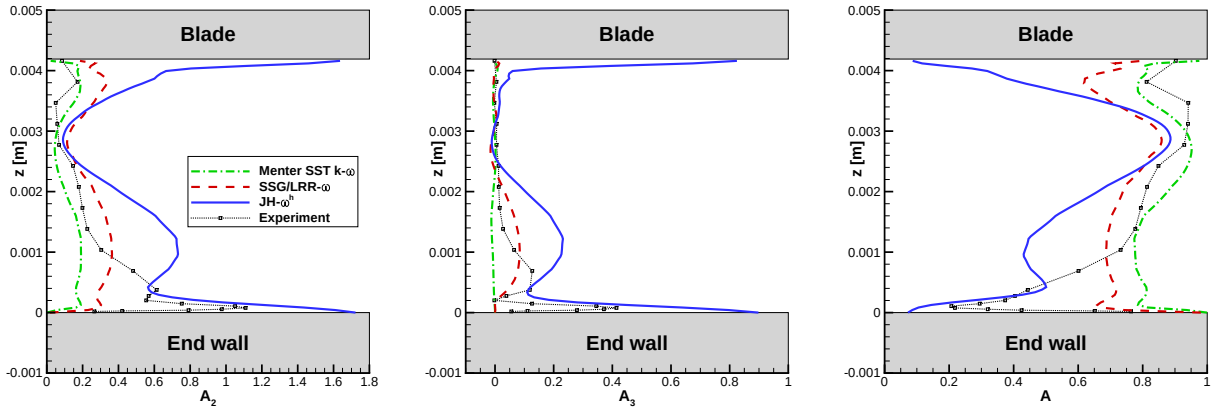

Figure 4: Reynolds stress anisotropy invariants in tip-gap at measurement position 5c.

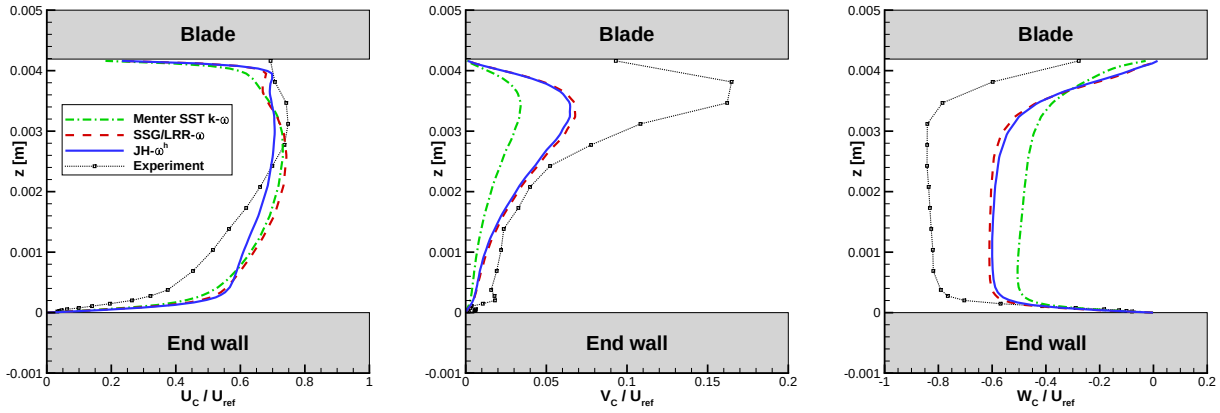

Figure 5: Velocity components in tip-gap at measurement position 5c.

show such a trend except for the points closest to the wall, whereas towards the blade tip wall, no such trend can be observed, suggesting that the velocities were possibly not measured down to the wall. It cannot be expected from the LEVM to correctly predict turbulence anisotropy but also the high Reynolds SSG/LRR-ω DRSM is not able to capture the peak of anisotropy at the end wall. The low Reynolds JH-ω^h DRSM formulation, on the contrary, predicts this peak in line with the channel flow results and displays the correct two-component turbulence behavior at both solid walls in the tip-gap. Below the blade-tip boundary layer, turbulence reaches a nearly isotropic state with $A \rightarrow 1$, which is predicted by both DRSMs.

The mean velocity is shown in a coordinate system aligned with the chord of the blade. U_C is in the direction of the chord, V_C points in the spanwise direction and W_C is the blade-to-blade direction. Figure 5 shows the mean velocity components in the specified coordinate system normalised by the inflow velocity U_{ref}. The measured velocities do not

vanish at the blade tip wall which is in line with the findings concerning the turbulence anisotropy. Whilst an almost symmetric chordwise velocity profile is predicted by the LEVM, experiments show a higher velocity near the blade tip than near the end wall. This asymmetry is predicted qualitatively by the JH-ω^h and partly by the SSG/LRR-ω DRSM. Furthermore, improvements of the results obtained with DRSMs as compared to LEVM results can be seen especially in the secondary flow directions. However, although the structure of the turbulence is predicted much better when DRSMs are employed, the improvement in quantitative agreement of mean velocity data is still far from optimal.

5 CONCLUSIONS

The flow in a low speed compressor cascade with tip-gap was simulated using DRSMs of different complexity. Whereas the SSG/LRR-ω model employs coefficients that are blended by a single empirical function, the JH-ω^h model introduces variable coefficients which are deduced from analysis of DNS data. Furthermore, the latter explicitly includes near-wall effects in the pressure-strain term and through the use of the specific homogeneous dissipation rate as scale determining variable. Improvements in the prediction of turbulence anisotropy could, therefore, be shown in the results obtained with the JH-ω^h compared to the SSG/LRR-ω DRSM. This is in agreement with the improved normal stress prediction in the turbulent plane channel flow. Improvements in mean velocity components, however, could be shown compared to the LEVM but were not as pronounced, both DRSMs showed similar behaviour.

This leads to the real dilemma of turbulence modelling. In order to gain insight into turbulence mechanisms and derive appropriate models, highly idealised flows focussing on very few isolated effects have to be studied: basically all turbulence models are calibrated using such flows. What distinguishes the various models is how accurately the flow features of building block flows can be reproduced. However, almost all flows to which the models are applied are highly complex and feature combinations of various effects. Since the governing equations are non-linear it can *per se* not be expected that a model calibrated for a number of idealised flows yields satisfying results in a complex flow. Nevertheless, this procedure seems to be the only viable way to derive and calibrate turbulence models.

In the present study, the JH-ω^h model appears to be clearly superior to the SSG/LRR-ω model in the prediction of the building block flow. Yet, this advantage cannot be recognised as pronounced in a complex 3D flow. This raises the question of the appropriate level of complexity of DRSMs for practical simulations of such flows. It can only be answered by means of further investigations, such as the analysis of turbomachinery components including rotating frames of reference, planned by the authors.

REFERENCES

[1] Gerolymos, G. A., Neubauer, J., Sharma, V. C., and Vallet, I., "Improved Prediction of Turbomachinery Flows Using Near-Wall Reynolds-Stress Model," *J. Turbomach.*,

Vol. 124, No. 1, 2002, pp. 86–99.

[2] Gerolymos, G. A. and Vallet, I., "Robust Implicit Multigrid Reynolds-Stress Model Computation of 3D Turbomachinery Flows," *J. Fluids Eng.*, Vol. 129, No. 9, 2007, pp. 1212–1227.

[3] Rautaheimo, P. P., Salminen, E. J., and Sikonen, T. L., "Numerical simulation of the flow in the NASA low-speed centrifugal compressor," *Int. J. Turbo Jet. Eng.*, Vol. 20, 2003, pp. 155–170.

[4] Borello, D., Hanjalić, K., and Rispoli, F., "Computation of tip-leakage flow in a linear compressor cascade with a second-moment turbulence closure," *Int. J. Heat Fluid Fl.*, Vol. 28, No. 4, 2007, pp. 587 – 601.

[5] Morsbach, C., Franke, M., and di Mare, F., "Towards the application of Reynolds stress transport models to 3D turbomachinery flows," *7th International Symposium on Turbulence, Heat and Mass Transfer*, Palermo, Sicily, Italy, Sept. 2012.

[6] Menter, F., Kuntz, M., and Langtry, R., "Ten years of Industrial experience with the SST model." *Turbulence, Heat and Mass Transfer 4*, edited by K. Hanjalić, Y. Nagano, and M. Tummers, 2003.

[7] Speziale, C. G., Sarkar, S., and Gatski, T. B., "Modelling the pressure-strain correlation of turbulence: An invariant dynamical systems approach," *J. Fluid Mech.*, Vol. 227, 1991, pp. 245–272.

[8] Launder, B. E., Reece, G., and Rodi, W., "Progress in the development of a Reynolds-stress turbulence closure," *J. Fluid Mech.*, Vol. 68, 1975, pp. 537–566.

[9] Eisfeld, B., "Reynolds Stress Modelling for Complex Aerodynamic Flows," *V European Conference on Computational Fluid Dynamics ECCOMAS CFD 2010*, Lisbon, Portugal, June 2010.

[10] Cécora, R.-D., Eisfeld, B., Probst, A., Crippa, S., and Radespiel, R., "Differential Reynolds Stress Modeling for Aeronautics," *50th AIAA Aerospace Sciences Meeting*, Nashville, TN, USA, Jan. 2012.

[11] Hanjalić, K. and Jakirlić, S., "Contribution towards the second-moment closure modelling of separating turbulent flows," *Comput. Fluids*, Vol. 27, No. 2, 1998, pp. 137 – 156.

[12] Jakirlić, S., *A DNS-based Scrutiny of RANS Approaches and their Potential for Predicting Turbulent Flows*, Habilitation, TU Darmstadt, 2004.

[13] Jakirlić, S. and Hanjalić, K., "A new approach to modelling near-wall turbulence energy and stress dissipation," *J. Fluid Mech.*, Vol. 459, 2002, pp. 139–166.

[14] Maduta, R. and Jakirlić, S., "Scrutinizing scale-supplying equation towards an instability sensitive Second-Moment Closure model," *8th International ERCOFTAC Symposium on Engineering Turbulence Modelling and Measurements - ETMM8*, Marseille, France, June 2010.

[15] Menter, F., "Improved Two-Equation k-ω Turbulence Models for Aerodynamic Flows," Technical Memorandum 103975, NASA Ames Research Center, Moffett Field, CA, USA, Oct. 1992.

[16] Becker, K., Heitkamp, K., and Kügeler, E., "Recent Progress In A Hybrid-Grid CFD Solver For Turbomachinery Flows," *V European Conference on Computational Fluid Dynamics ECCOMAS CFD 2010*, Lisbon, Portugal, June 2010.

[17] Morsbach, C. and di Mare, F., "Conservative segregated solution method for turbulence model equations in compressible flows," *6th European Congress on Computational Methods in Applied Sciences and Engineering (ECCOMAS 2012)*, Vienna, Austria, Sept. 2012.

[18] Fiedler, J. and di Mare, F., "Generalised Implementation Of Low-Mach Preconditioning For Arbitrary Three-Dimensional Geometries," *6th European Congress on Computational Methods in Applied Sciences and Engineering (ECCOMAS 2012)*, Vienna, Austria, Sept. 2012.

[19] Schumann, U., "Realizability of Reynolds-stress turbulence models," *Physics of Fluids*, Vol. 20, No. 5, 1977, pp. 721–725.

[20] Kim, J., Moin, P., and Moser, R., "Turbulence statistics in fully developed channel flow at low Reynolds number," *J. Fluid Mech.*, Vol. 177, 1987, pp. 133–166.

[21] Hoyas, S. and Jimenez, J., "Scaling of the velocity fluctuations in turbulent channels up to $\mathrm{Re}_\tau = 2003$," *Phys. Fluids*, Vol. 18, No. 1, 2006, pp. 011702.

[22] Hanjalić, K. and Jakirlić, S., "A model of stress dissipation in second-moment closures," *Apl. Sci. Res.*, Vol. 51, 1993, pp. 513–518, 10.1007/BF01082584.

[23] Muthanna, C., *The Effects of Free Stream Turbulence on the Flow Field through a Compressor Cascade*, Dissertation, Virginia Polytechnic Institute and State University, 2002.

[24] Tang, G., *Measurements of the Tip-Gap Turbulent Flow Structure in a Low-Speed Compressor Cascade*, Dissertation, Virginia Polytechnic Institute and State University, 2004.